UV climatology at Palmer Station, Antarctica, based on Version 2 NSF network data

Germar Bernhard*, Charles R. Booth**, James C. Ehramjian***

Biospherical Instruments Inc., San Diego

ABSTRACT

Spectral ultraviolet (UV) and visible irradiance has been measured at Palmer Station, Antarctica, between 1988 and 2004 with a SUV-100 spectroradiometer. The instrument is part of the U.S. National Science Foundation's UV Monitoring Network. Here we present a UV climatology for Palmer Station based on the recently produced "Version 2" data edition. This data set will supersede the original release "Version 0". Corrections applied to the new version increased biologically effective UV dose rates by 0-9%. Values of UV-A irradiance changed by –8% to +10%. A comparison with results of a radiative transfer model confirmed that measurements of different years are consistent to within ±5%. Total ozone column was calculated from UV spectra and was found to agree with measurements of NASA's Total Ozone Mapping Spectrometer (TOMS) installed on the Nimbus-7 satellite to within 1%. TOMS measurements on the Earth Probe satellite are 3% lower than SUV-100 data. Effective surface albedo was estimated from clear sky spectra. Between August and November, albedo typically ranges between 0.6 and 0.95. After melting of snow and sea ice, albedo varies between 0.3 and 0.5. Biologically effective UV radiation is largest in November and December when low total ozone amounts coincide with relatively small solar zenith angles (SZA). During these months, the noon-time UV Index typically varies between 4 and 7, but UV indices as high as 14.8 have been observed. The largest erythemal daily dose of 8.8 kJ/m² was measured on 11/10/97 and 12/7/98. Linear regression analyses did not indicate statistically significant trends in UV or visible radiation, with the exception of February when small downward trends with statistical significance were observed. On average, clouds reduce UV irradiance at 345 nm between 28% (October and November) and 42% (February) compared to clear sky levels. In extreme cases, reductions by clouds can be as high as 90%. Between September and November, the variability introduced by ozone is similar to that caused by clouds.

Keywords: Solar ultraviolet radiation, Antarctica, climatology, total ozone, albedo.

1. INTRODUCTION

The National Science Foundation's Office of Polar Programs (NSF/OPP) UV Monitoring Network was established in 1987 in response to severe ozone depletion reported in Antarctica. Biospherical Instruments (BSI) installed the first instruments in 1988[1] and has operated the network since.[2] The network currently consists of seven sites, which are mostly located at high latitudes. All stations measure global spectral irradiance between 280 and 600 nm with high-resolution SUV-100 and SUV-150B spectroradiometers. Further information on the network and its data is available at the website www.biospherical.com/nsf.

Currently published network data are based on the originally released "Version 0" data set. This data set has not been corrected for deviations of the angular response of SUV-100 spectroradiometers from the ideal cosine response nor for wavelength errors of approximately 0.1 nm, which affect spectra measured before 1997. To improve the accuracy and homogeneity of network data, a new data edition named "Version 2" is currently being generated. Version 2 data are not "pure" measurements like Version 0 data, as radiative transfer calculations are used for the various corrections. These model calculations also provide clear-sky reference spectra during cloudy periods. Version 2 data from the instrument located at the South Pole (SPO) and McMurdo (MCM) were recently introduced.[3,4] Here we present the new Version 2

* bernhard@biospherical.com; phone 1 619 686-1888; fax 1 619 686-1887; http://www.biospherical.com; Biospherical Instruments Inc., 5340 Riley Street, San Diego, CA 92110-2621, USA; ** booth@biospherical.com; *** jime@biospherical.com

Ultraviolet Ground- and Space-based Measurements, Models, and Effects V,
edited by G. Bernhard, J. R. Slusser, J. R. Herman, W. Gao, Proc. of SPIE Vol. 5886
(SPIE, Bellingham, WA, 2005) · 0277-786X/05/$15 · doi: 10.1117/12.614172

data set for the network instrument installed at the U.S. base Palmer Station (PAL), located on Anvers Island next to the Antarctic peninsula.

The UV climate at PAL differs in several ways from that at SPO and MCM: PAL is located at the lowest latitude of the three Antarctic sites. This leads to larger solar elevations and larger UV levels. Large changes in total column ozone during the annually recurring "ozone hole" are observed depending on the location of the polar vortex. Radiation levels in late November and early December can exceed those observed during summer in San Diego, California (33°N) when small stratospheric ozone amounts coincide with relatively small solar zenith angles. Clouds are more frequent and have a larger optical depth compared to the other two Antarctic network sites. Surface albedo shows a large change over the year with highest values in winter when the ocean adjacent to the station is frozen. During summer, the ocean is mostly ice free, but icebergs and drift ice can be blown in at any time. Temperatures in summer are frequently above 0°C, and rain is not uncommon. The UV climate is further influenced by the complicated topography and mix of surface conditions around the station, including open ocean, mountains, glaciers, and dark rock.

2. DATA ANALYSIS

2.1 Measurements

Measurements of global spectral irradiance were performed at building T5 at Palmer Station (64°46' S, 64°03' W, 21 m above sea level) between March 1990 and May 2004 with a SUV-100 spectroradiometer from BSI. The instrument is mounted into the roof of a building and measures solar spectra between 280 and 600 nm with a resolution of approximately 1.0 nm at a rate of 4 spectra per hour (1 spectrum per hour prior to 1997). Palmer Station is surrounded by ocean to the west and south and the Marr Ice Piedmont glacier to the east and north. The surface in the immediate vicinity of the instrument are dark rocks, which are covered by snow between April and December.

2.2. Radiative transfer calculations

Measurements were complemented with model calculations performed with the radiative transfer model UVSPEC/libRadtran Version 1.01, available at www.libradtran.org.[5] The model's double-precision pseudospherical disort radiative transfer solver with six streams and 50 layers was used.

The extraterrestrial spectrum (ETS) used for modeling is based on the ETS recently proposed by Gueymard.[6] Since the resolution of this spectrum is not sufficient to be used directly in the model, we superimposed the fine structure from the "Kitt Peak solar flux atlas".[7] The composite spectrum is identical with the spectrum $E_{\mathrm{Gueymard}}(\lambda)$ introduced in Ref. 3. Air density and pressure profiles were taken from Anderson.[8] Surface pressure was provided by the University of Wisconsin-Madison. Total column ozone was calculated from measured UV spectra as described in Section 2.3. Ozone and temperature profiles were derived from ozone sonde observations performed at the Argentine research station Marambio (64°15' S, 56°39' W). Only profiles with a burst altitude of at least 30 km were used, and profiles were extrapolated to higher altitudes using an algorithm described by Bernhard.[9] We calculated the total ozone column from these profiles and selected those profiles for modeling whose total ozone amounts best matched the total ozone column observed by TOMS on the day of UV measurements.

Effective surface albedo was calculated from UV spectra measured during clear skies as described in Section 2.6 and interpolated to times of cloudy days. During longer periods of persistent cloudiness, also snow depth measurements provided by the University of Wisconsin-Madison were used to estimate albedo. Aerosol extinction was parameterized with Ångström's turbidity formula by setting the Ångström coefficients α and β to 1.0 and 0.0125, respectively. The resulting aerosol optical depth (AOD) at 500 nm is 0.025. This value is in agreement with measurements by Shaw,[10] who determined background AOD at the Antarctic coast to $\tau=0.025\pm0.010$. Modeled spectra were convolved with a triangular function of 1.0 nm full width at half maximum (FWHM). Clear-sky spectra were selected from the data set based on temporal variability of spectral irradiance at 600 nm using a similar method as described in Ref. 3.

2.3. Calculation of total column ozone and comparison with TOMS observations

Total column ozone was calculated from measured UV spectra using the inversion algorithm described by Bernhard,[11] the Bass and Paur[12] ozone absorption cross section, and ozone and temperature profiles introduced in Section 2.2. The ozone value returned by the algorithm was used for modeling. Figure 1 shows a comparison of these total ozone values with Version 8 overpass ozone data from NASA's Total Ozone Mapping Spectrometers (TOMS) installed on Nimbus-7 and Earth Probe satellites. The ratio TOMS Nimbus-7 / SUV-100 calculated from data of the period March 1990 – May 1993 is 0.991±0.061 (±1σ); the ratio TOMS Earth Probe / SUV-100 calculated from the period July 1996 – December 2000 is 0.970±0.059. Data after December 2000 were not used due to the recent degradation of the Earth Probe TOMS front scan mirror (personal communication with R.D. McPeters, NASA). The comparison only slightly depends on SZA and total ozone, although the ratio TOMS / SUV-100 is slightly smaller when total ozone is low. We used our ozone data for modeling as they are available for every day with spectral measurements.

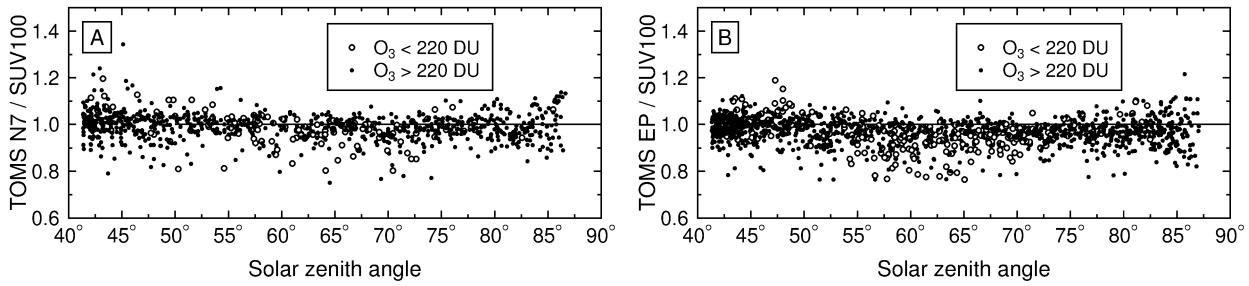

Figure 1. (A) Ratio of TOMS Nimbus-7 and SUV-100 total ozone data from the period March 1990 – May 1993. (B) Ratio of TOMS Earth Probe and SUV-100 total ozone data from the period July 1996 – December 2000.

2.4. Corrections applied to Version 2 data

Wavelength shifts have been corrected by correlating the Fraunhofer line structure in measured spectra to the corresponding structure in modeled spectra as described in Ref. 3. Residual wavelength uncertainties after correction are on average ±0.04 nm (±1σ) at 305 nm, and ±0.03 nm at longer wavelengths. Corrections for the cosine error of the SUV-100 spectroradiometer have been performed with the method described in Ref. 3. These corrections pose a challenge as characterizations of the error prior to deployment of the SUV-100 proved to be not applicable to the assembled and installed instrument. Solar data further suggest that the error depended on azimuth angle and wavelength prior to a modification of the instrument's irradiance collector in March 2000. The error has also changed when the instrument was serviced. This results in relatively large uncertainties of the correction, particularly at large SZA. The bandwidth of SUV-100 spectroradiometers varies between 0.9 and 1.1 nm in the UV-B and 0.7 and 0.9 nm in the visible. Processing of Version 2 data involved normalization of all spectra to a uniform bandwidth of 1.0 nm and resampling of spectra to uniform wavelength step intervals.

2.5. Uncertainty budget

A detailed analysis of the uncertainty of Version 2 data from Palmer Station is available at the Version 2 website at www.biospherical.com/nsf/version2. For spectral irradiance at 310 nm, uncertainties at the 2σ-level (equal to a coverage factor of k=2) range between 6.2% and 6.4% and are dominated by uncertainties related to calibration, stability, and wavelength errors. At longer wavelengths, the overall uncertainty is governed by the uncertainty of the cosine error correction. This is a problem particularly during periods of varying cloudiness. Under overcast conditions, the 2σ-uncertainty for spectral irradiance is 6.4% at 310 nm and 4.6% at 400 and 600 nm. Under variable cloud conditions, when it cannot be determined whether the disk of the Sun is visible or not, expanded uncertainties can be as high as 13% at 600 nm. Expanded uncertainties for erythemal irradiance (i.e. spectral irradiance weighted with the CIE action spectrum for sunburn[13]) and DNA-damaging irradiance (action spectrum by Setlow[14]) range between 5.6% and 6.4%, and are only slightly influenced by sky condition.

2.6. Calculation of effective albedo

Effective albedo is defined as the albedo of a uniform Lambertian surface, that, when used as input into a 1-D model, reproduces the measured spectrum.[15] Albedo leads to a wavelength-dependent increase in surface UV with larger changes at shorter wavelengths. Utilizing this principle, effective albedo was calculated from clear-sky UV spectra with the method described in Ref. 4. The 1σ-uncertainty of the retrieved albedo value is about 0.1. However, larger errors may occur if spectra contaminated by clouds are mistakenly used in the retrieval. This is a problem at Palmer Station where clear sky conditions are rare.

Figure 2A shows effective albedo values calculated from all available clear-sky spectra measured at PAL between March 1990 and May 2004 for SZA smaller than 80°. Between August and November, albedo values typically range between 0.6 and 0.95. After snowmelt, albedo varies between 0.3 and 0.5. Effective albedo does not fall below 0.25 due to the glaciers surrounding PAL. Figure 2A also shows reflectivity data extracted from TOMS Nimbus-7 and Earth Probe overpass data for times coinciding with SUV-100 albedo values. These values exhibit a large variation between 0.06 and 0.82 and do not agree well with SUV-100 data. Part of this discrepancy is caused by the complex topography and rapidly changing surface conditions in the vicinity of the instrument and the fact that TOMS reflectivity is the average over an area of 50 × 50 km^2. For example, there may be occasions when TOMS "sees" only open water within its pixel (resulting in a low reflectivity measurement) and dose not see the influence of the glacier next to the instrument. The correlation between TOMS reflectivity and effective albedo is presented in more detail in Figure 2B. After snow melt, when effective albedo varies between 0.3 and 0.5, TOMS reflectivity ranges between 0.06 and 0.8. When effective albedo is larger than 0.5, there is a reasonable correlation between albedo and TOMS reflectivity, although TOMS measures on average lower by approximately 0.15.

Albedo values used for modeling of Version 2 spectra during cloudy periods were interpolated from the clear-sky data set and also estimated from snow depth, measured by the University of Wisconsin. The interpolated values have larger (but difficult to quantify) uncertainties, in particular during long-lasting periods of persistent cloudiness.

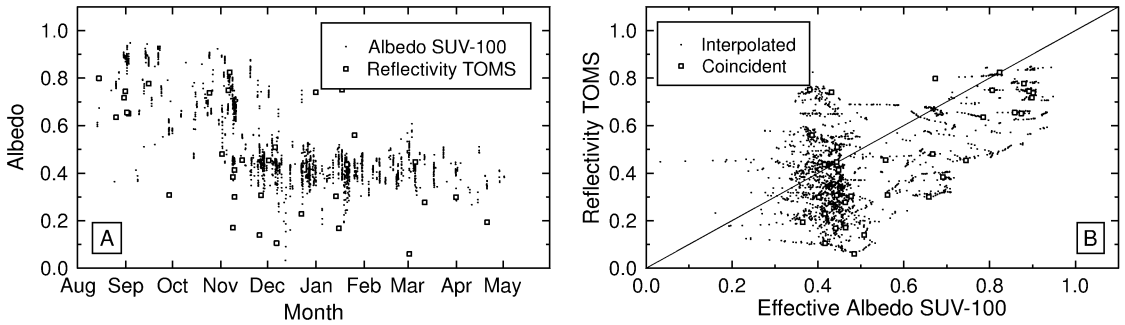

Figure 2. (A) Effective albedo calculated from SUV-100 spectra sampled during clear skies and reflectivity measurements from TOMS at Palmer Station. (B) Correlation between TOMS reflectivity and effective albedo. The "interpolated" data set was interpolated from the daily TOMS observation to the time of SUV-100 measurements. The "coincident" data set includes TOMS observations within ±15 minutes of the SUV-100 measurements.

2.7. Comparison of Version 0 and Version 2

Version 2 data were compared with the original release "Version 0". A detailed comparison of the two versions is available on the Version 2 website at www.biospherical.com/nsf/Version2, focusing on nine spectral intervals in the UV and visible as well as erythemal[13] and DNA-damaging[14] irradiance. Differences are mostly caused by wavelength error and cosine error corrections. Differences between 300 and 310 nm range between –2% and +20% and are predominantly caused by difference in the wavelength calibrations of the two versions. Above 310 nm, the difference of the two versions is due to the cosine error correction and the way spectra are constructed from the underlying raw-data. Differences between Version 0 and 2 peak at SZAs between 65° and 80°, depending on the spectral band. Erythemal

and DNA-damaging dose rates from the Version 2 data set are between 0 and 9% higher than Version 0 data. The differences depends on SZA, year, and sky condition, amongst other causes. Differences for UV-A irradiance range between –8% and +10%. Differences for the integral between 400 and 600 nm range between 0% and +20%. Ratios of Version 2 and Version 0 data show a somewhat different pattern before and after March 2000, when the instrument's collector was modified.

2.8. Self-consistency of Version 2 data

After Version 2 data were produced, the consistency of the new data set was examined by comparing clear-sky measurements of different years. In the first step of the analysis, the ratio $q_{V2}(\lambda) \equiv E_M(\lambda) / E_C(\lambda)$ of measured spectra $E_M(\lambda)$ and modeled spectra $E_C(\lambda)$ was calculated from all data associated with clear-sky periods. The comparison with the model is helpful to remove the dependence of known parameters such as SZA, total ozone, and albedo from the measurement, which are different every year. It also alleviates the difficulty that clear skies occur in different periods for every year. Note that model results were part of the correction procedures used to generate Version 2 data. For example, total ozone and albedo were retrieved from measured spectra and used as model input parameters. Model results are therefore not independent from the measurement. Nonetheless, a comparison of measurement and model proved to be valuable in detecting problems of the measurements.

In the second step of the analysis, medians of $q_{V2}(\lambda)$ were calculated for every year on a wavelength-by-wavelength basis using all available ratio spectra $q_{V2}(\lambda)$ with SZA smaller than 75°. The resulting median-ratio-spectra are denoted $M(\lambda, y)$ and vary between 0.95 and 1.05 for wavelengths larger than 320 nm. For the final step of the analysis, we consider the ratio $Q(\lambda, y)$, defined as:

$$Q(\lambda, y) = \frac{M(\lambda, y)}{\frac{1}{11} \sum_{y'=1994}^{2004} M(\lambda, y')} . \quad (1)$$

The denominator of Eq. (1) is the average of all median-ratio-spectra from 1994 – 2004, which are years with background aerosol conditions. Due to the construction of $Q(\lambda, y)$, systematic differences between measurement and model, which affect all years equally such as those arising from the ETS used by the model, are ratioed out. These "Q-ratios" are shown in Figure 3 for every year. With the exception of 1990, Q-ratios of all years agree to within ±5% confirming that corrected measurements of all years but 1990 are consistent at the ±5% level and agree within the measurement uncertainty. Measurements from 1990 mark the start of operational measurements at PAL. At that time, neither calibration procedures nor calibration standards were as well established as in later years of operation. In addition, the determination of the median $M(\lambda,1990)$ is uncertain since it is based on 12 ratio-spectra only due to the lack of sufficient clear sky data.

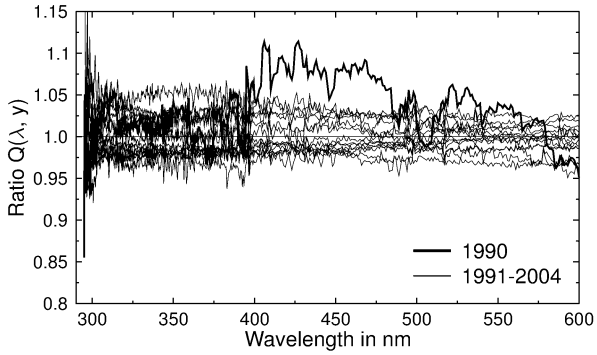

Figure 3. Normalized Q-ratios of measurement and model for the years 1990 - 2004. A color version of the plot is available at www.biospherical.com/NSF/Version2.

4. UV CLIMATOLOGY AT PALMER STATION

4.1. Time series and trends

After Version 2 data for PAL had been generated, the data set was used to establish a climatology of ultraviolet and visible radiation. Figure 5 shows time-series of daily doses of four Version 2 data products for the period March 1990 – May 2004. Daily doses were calculated by integrating instantaneous measurements of the four data products over 24 hour periods. Gaps in time series of two hours or less were filled via spline interpolation. Days with gaps longer than two hours were excluded from further analysis. The four data products are spectral irradiance at 305 nm, erythemal irradiance[13], spectral irradiance integrated over 342.5 to 347.5 nm, and spectral irradiance integrated over 400 to 600 nm. Figure 4 also shows daily doses of short-wave irradiance (0.3-3.0 μm) measured by a pyranometer. Daily doses measured in different years on the same calendar day were averaged to setup a climatology. These climatological mean values are indicated by thin lines in Figure 4 for all five data products. Clear sky model values are also indicated.

Figure 4 supports the following conclusions:

- In some years, daily doses of the spectral irradiance at 305 nm show large deviations from the climatological mean, in particular during the months September – December, which are affected by the ozone hole. High values were more frequent in the years 1993 – 1998 than during 2000 – 2004.
- Daily erythemal doses show a similar pattern as the 305-nm dose, but variability and relative departures from the climatological mean are generally smaller. This can be expected since erythemal irradiance is less sensitive to changes in atmospheric ozone amounts than spectral irradiance at 305 nm. The largest erythemal daily dose was 8.8 kJ/m², measured on 11/10/97 and 12/7/98.
- Daily doses calculated from the integral 342.5–347.5 nm are not sensitive to changes in total ozone. The large variability is mostly caused by changes in cloud cover and to a lesser extent by variations in albedo. Measured daily doses are generally below daily doses calculated with the radiative transfer model for clear skies.
- Daily doses calculated from the integral 400–600 nm and from pyranometer measurements exhibit a similar pattern as that of daily doses for the 342.5–347.5 nm integral. However, variability generally increases with increasing wavelength.

In order to quantify long-term changes, we calculated monthly averages of the daily doses depicted in Figure 4. Only months with at least 25 daily dose values were used for further analysis. Figure 5 shows the resulting time series of monthly average daily doses of the four SUV-100 data products and the short-wave data set. Trend lines were calculated for all data sets by linear regression and are also shown in Figure 5. Slopes of the trend lines (expressed in change per decade relative to the year 1990), their 2σ-uncertainty, and regression coefficients R^2 are given in the figure's legend.

Trends vary between –29% and +20% per decade, depending on data product and month, but are generally not significant at the 2σ level. One exception is the month of February, which shows slightly significant trends of –11% and –10% for irradiation at 305 nm and erythemal dose, respectively. For the other months, the large inter-annual variability in ozone and cloud cover obscures any trend, if it exists.

Average monthly doses calculated from spectral irradiance at 305 nm and erythemal irradiance exhibit large year-to-year variability during September and December as atmospheric ozone concentrations fluctuate substantially from year to year. For these two data products, monthly doses for November were substantially larger between 1993 and 1997, than during more recent years. Monthly doses of these two data products are also frequently larger in November than December, indicating that the effect of the smaller SZA in December is offset by lower total ozone values in November.

Monthly average doses for the 342.5-347.5 nm and 400-600 nm integrals show less variability from year to year than doses of data products sensitive to atmospheric ozone concentrations. The inter-annual pattern of the 400-600 nm dose is very similar to that of short-wave dose. For example, data from January 1993 are high in both data sets and data from November 1992 are low. Version 2 data from the SUV-100 are independent from the pyranometer measurements. The good agreement of the two data sets reassures the quality of measurements of both instruments.

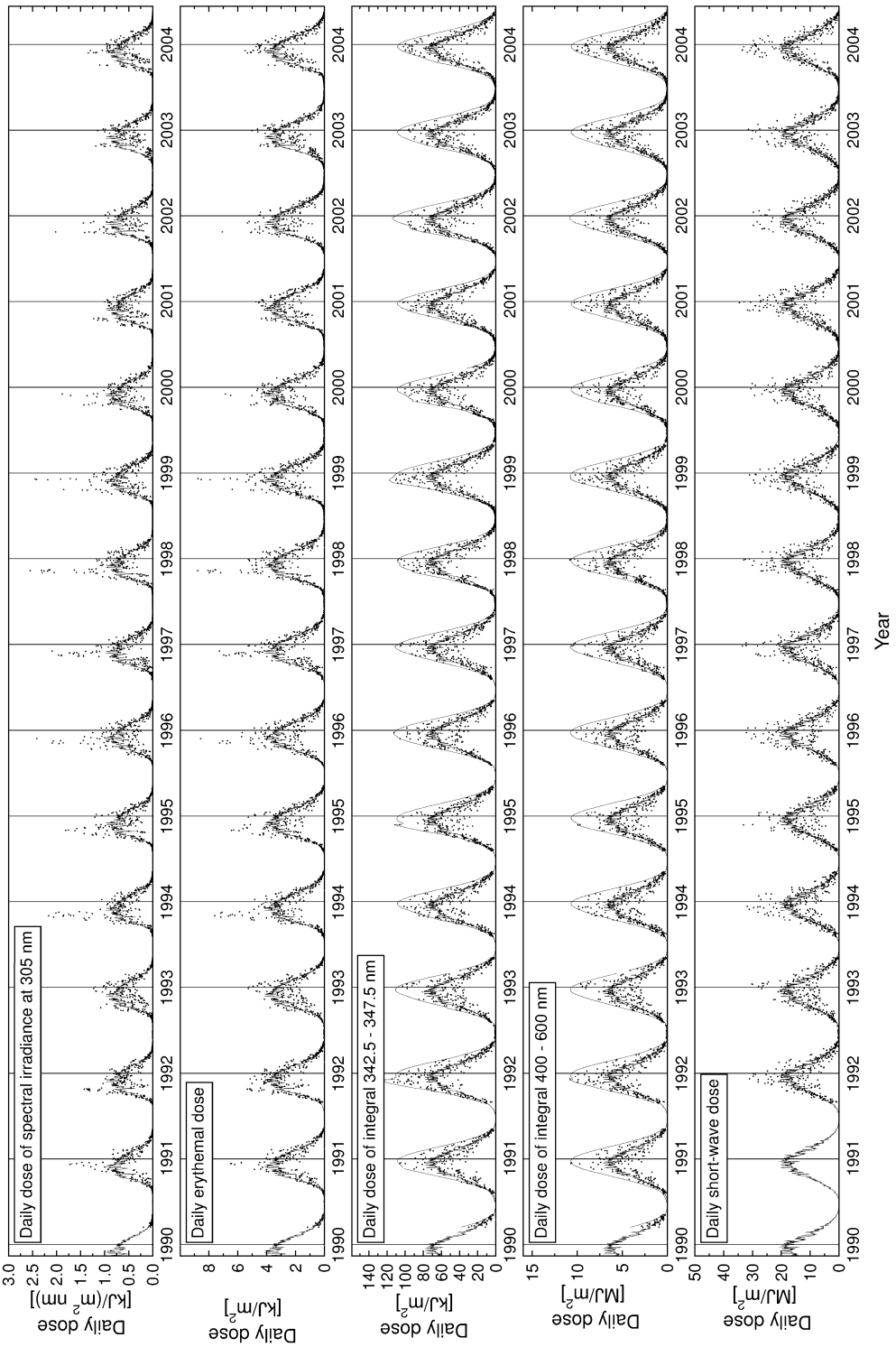

Figure 4. Time series of daily dose of the data products spectral irradiance at 305 nm, erythemal irradiance, integral of 342.5-347.5 nm, integral 400-600 nm, and daily short-wave dose at Palmer Station. Lines plotted in all panels indicate the climatology, calculated by averaging measurements of all years. Additional thin line in the panels of the integrals 342.5 – 347.5 nm and 400 – 600 nm were calculated by the clear-sky model. These model calculations differ slightly from year to year due to variations in albedo. A color version of the plot is available at www.biospherical.com/NSF/Version2.

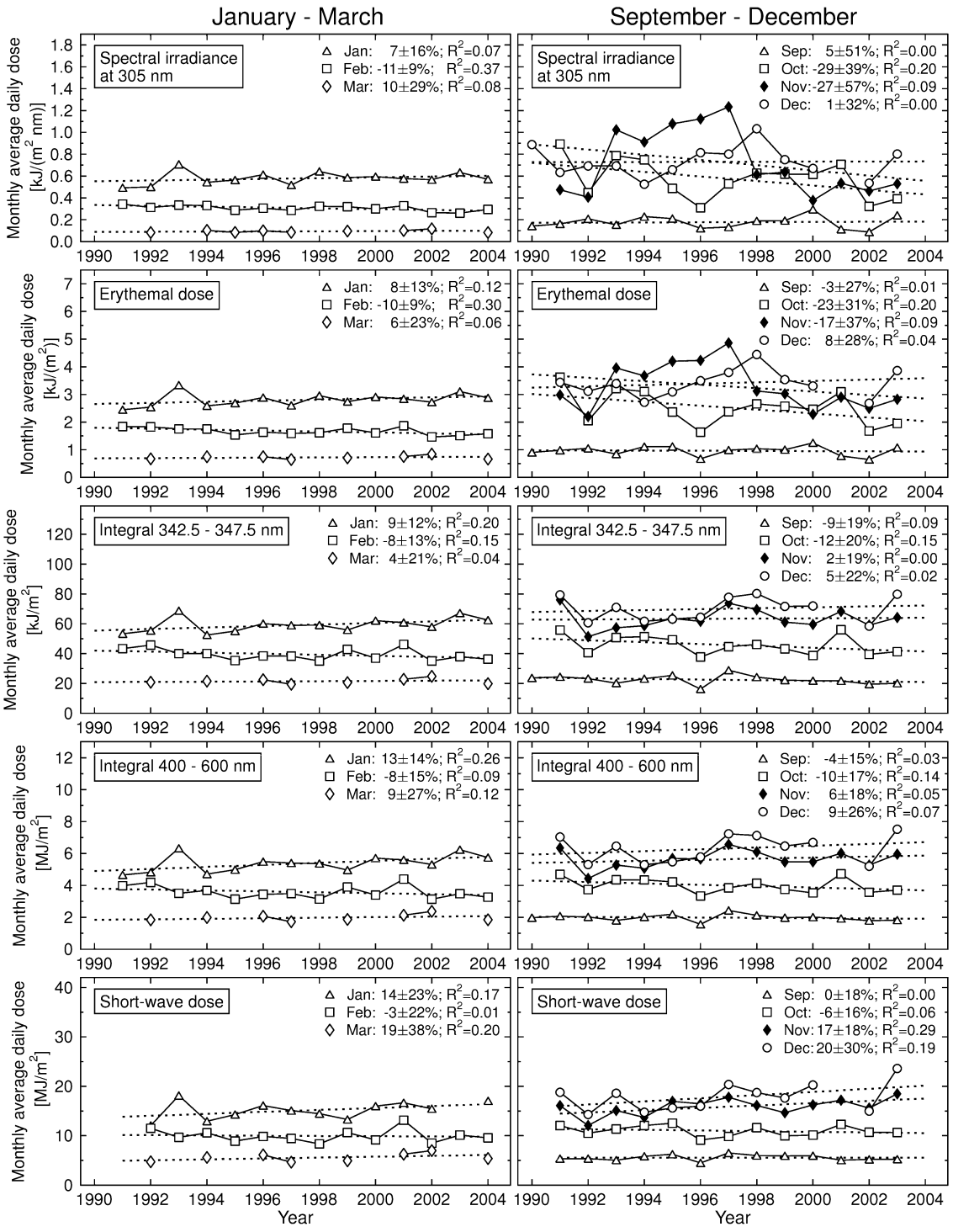

Figure 5. Time series of average monthly daily dose for the months of January – April (left column) and September – December (right column) for five data products, indicated in the top left corner of each plot. Dashed lines are trend lines determined by linear regression. Trend per decade relative to 1990, 2σ-uncertainty of trend, and regression coefficient R^2 are also indicated.

A similar analysis based on noon-time irradiance instead of daily dose is available at the Version 2 website at www.biospherical.com/NSF/Version2. Observed trends for noon-time irradiance are very similar to those found in daily doses. Typical noon-time UV Indices in November and December vary between 4 and 7, but larger values have been observed when low total ozone amounts occur late in the year when prevailing SZAs are small. The largest UV Index[13] was 14.8 and was measured on 12/4/98.

6.2. Effect of clouds and albedo on UV

Clouds are the dominant factor in reducing UV radiation below clear-sky level. In a high-albedo environment, the effect of clouds is substantially modified by surface albedo.[16,17] The effects of cloud and albedo are therefore discussed together.

The modification of UV radiation by the combined effects of clouds and albedo was quantified with transmittance $T(t)$, defined as

$$T(t) = \frac{E_{M,345}(t)}{E_{C,345}(t)} \Bigg/ \sum_{\tilde{t} \in y(t), p_i(t), \mathrm{CS}} \frac{1}{n} \frac{E_{M,345}(\tilde{t})}{E_{C,345}(\tilde{t})}. \tag{2}$$

$E_{M,345}(t)$ is the measured Version 2 342.5-347.5 nm integral at time t, and $E_{C,345}(t)$ is the associated clear-sky model value. The denominator of Eq. (2) is the average ratio of measurement and model for clear sky conditions (CS) during year y and a two-week period p_i (1-January – 15-January, 16 January – 31 January, … 16-December – 31-December). This term removes the observed bias between measurement and model for clear skies in any given year and period. Corrections vary between 0.93 and 1.04; the average correction is 0.98. Albedo used for the calculation of $E_{C,345}(t)$ was determined from clear-sky spectra as described in Section 2.6. In the next step, $T(t)$-values for the period 1-Jan – 15-Jan and SZA < 75° were selected from data of all years, and binned into 0.02-wide intervals to set up a frequency distribution. Similar distributions were constructed for each period p_i and are shown in Figure 6. Each plot in this figure represents the climatology of transmittance relative to clear sky for a different part of the year.

Distributions of many periods display a distinct maximum at $T(t) = 1$, marking clear-sky conditions. Most distributions have a secondary maximum at $T(t) < 1$ related to the most likely transmittance under cloudy conditions. Average T-values vary between 0.57 and 0.78, depending on month. Minimum ratios may be as low as 0.1. This is significantly lower than minimum transmittances observed at the SPO and MCM. Enhancement of radiation beyond the clear sky value may exceed 15%. A similar analysis for the 400-600 nm integral can be found at the Version 2 website. These distributions are qualitatively similar to the distributions for the 342.5-347.5 nm integral, but confirm that the effect of clouds is larger in the visible than for the UV: average $T(t)$-values may be as low as 0.51. Some rationale for the increased effect of clouds at longer wavelengths is presented in Ref. 3.

6.3. Variability in UV due to variations in total ozone

The influence of total ozone on UV depends strongly on wavelength and therefore has to be evaluated separately for each wavelength or UV data product of interest. Here we focus on the UV Index, denoted $E_{M,\mathrm{UVI}}(t)$. To reduce the effect of clouds, we divided $E_{M,\mathrm{UVI}}(t)$ by $E_{M,345}(t)$ as discussed in more detail in Ref. 3:

$$\tilde{E}_{M,\mathrm{UVI}}(t) = E_{M,\mathrm{UVI}}(t) / E_{M,345}(t). \tag{3}$$

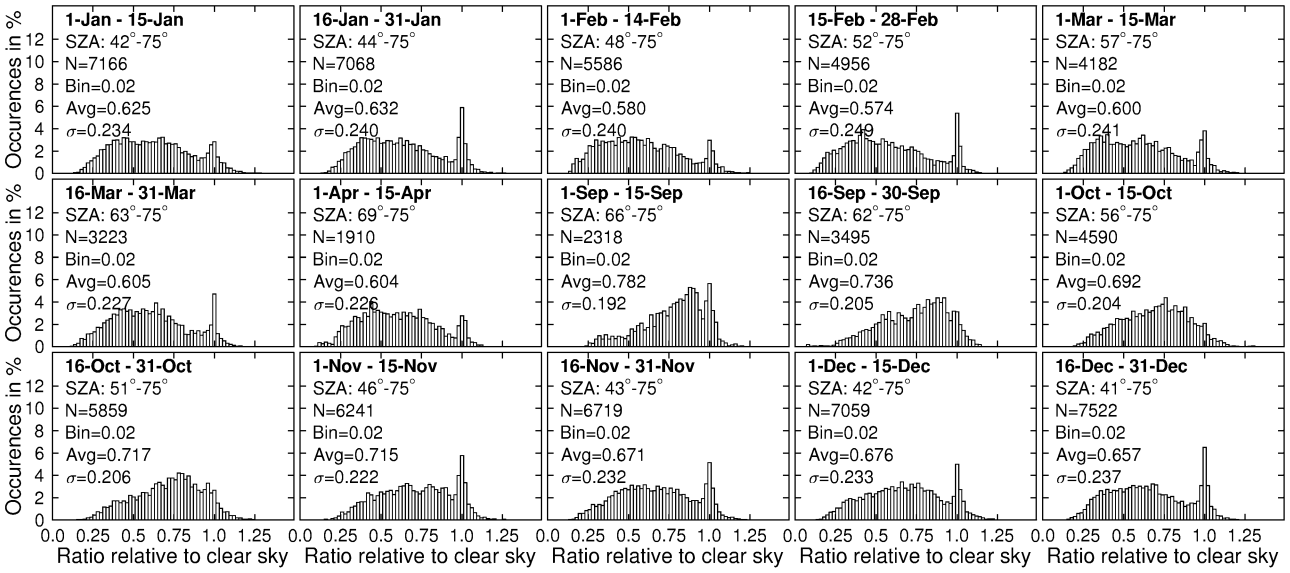

Figure 6. Frequency distributions of transmittance $T(t)$ defined as the ratio of spectral irradiance integrated over 342.5–347.5 nm to the associated clear sky irradiance, calculated from measurements of all years. Each of the 15 plots refers to a different two-week period as indicated in the top left corner of each plot. SZA-range, number of data points N, width of the histogram columns (Bin), average (Avg), and standard deviation (σ) of the distributions are also provided.

To quantify the year-to-year variability of $\widetilde{E}_{M,\mathrm{UVI}}(t)$, we selected data from different years that were measured at the same day and hour, and calculated their average. The ratio of individual measurements to this average is then used to describe inter-annual variability. The ratio is denoted $V_{\mathrm{UVI}}(t)$, and formally defined as:

$$V_{\mathrm{UVI}}(t,y) = \frac{\widetilde{E}_{M,UVI}(t,y)}{\frac{1}{n}\sum_{y'\in[1990,2004]} \widetilde{E}_{M,UVI}(t,y')}, \tag{4}$$

where t is time within a given year y. $V_{\mathrm{UVI}}(t)$ values are used for further analysis only if data from at least 8 years contribute to the average.

Similar to the approach described in Section 6.2., we constructed frequency distributions for $V_{\mathrm{UVI}}(t)$ using data from all years and 0.05-wide bins. The distributions are presented in Figure 7. Distributions for January – April are considerably narrower than distributions for September – December. Standard deviations of the distributions vary between 0.08 and 0.1 for January – April and between 0.31 and 0.34 for October and November. Thus, the variability is about three times as high in the austral spring compared to the first half of the year. The broader distributions are mainly caused by the influence of the ozone hole, which typically disappears sometime during the period of late November to the beginning of December.[18] A comparison of Figures 6 and 7 (and in particular the standard deviations of the distributions) suggests that during the first half of the year, the variability in UV introduced by clouds and albedo is about 2.5 times as high as that introduced by ozone. Between September and November, the variability introduced by ozone is comparable to that caused by clouds.

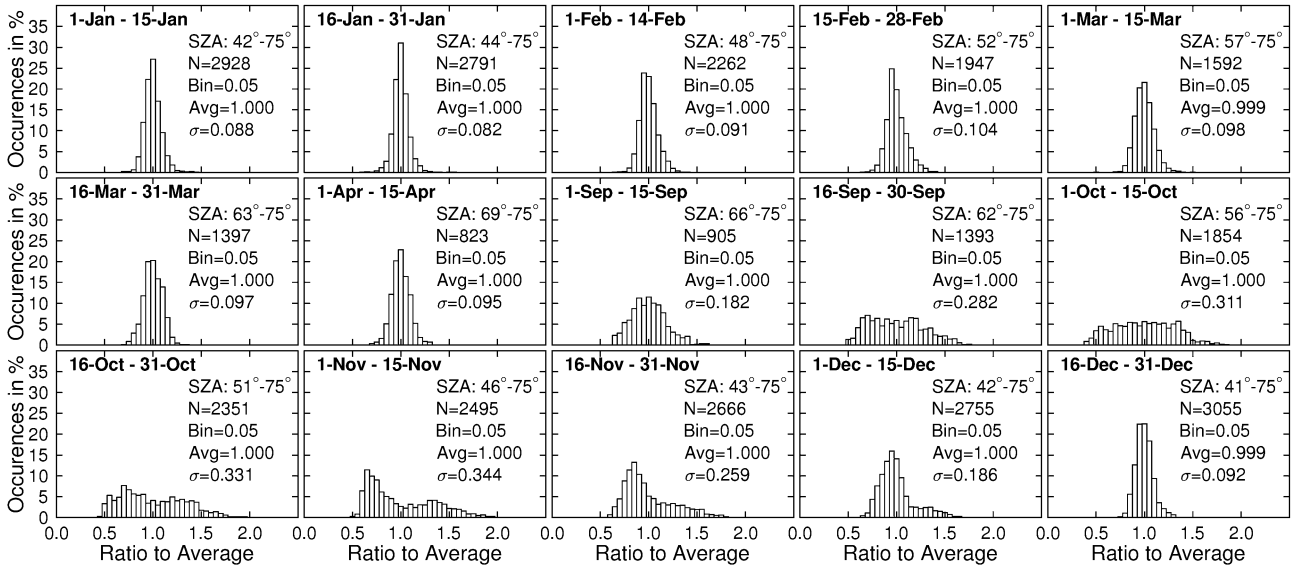

Figure 7. Frequency distribution of $V_{\mathrm{UVI}}(t)$ describing the variation of UV Index with respect to the average UV Index of the years 1990-2004. Each of the 15 plots refers to a different two-week period as indicated in the top left corner of each plot. SZA-range, number of data points N, width of the histogram columns (Bin), average (Avg), and standard deviation (σ) are indicated for every distribution.

5. DISCUSSION AND CONCLUSIONS

Version 2 data from the NSF/OPP UV spectroradiometer at PAL have been produced and feature smaller uncertainties and a larger number of data products than the original release "Version 0". New products include (but are not limited to) total ozone column and effective albedo for clear skies. Erythemal and DNA-damaging dose rates from the Version 2 data set are higher by 0-9% than Version 0 data. Clear sky measurements of different years typically agree to within ±5%. A climatology of UV radiation at PAL was established, focusing on changes in UV observed over time, the effect of clouds, and the variability introduced by total ozone fluctuations.

Daily doses of spectral irradiance at 305 nm and daily erythemal doses are largest in November when low ozone columns coincide with relatively small SZAs. Linear regression analyses of monthly average daily doses did not indicate statistically significant trends for any month but February where a downward trend of approximately 10% per decade was observed at all wavelengths. UV levels in November were considerably higher between 1993 and 1997 than in more recent years. This is consistent with measurements at SPO[3] and MCM,[4] and also with emerging evidence that ozone depletion may have reached its peak in the late nineties of the 20th century and the first years of the 21st century, and is now starting to recover.[19] However, it is too early to draw final conclusions considering that only the last five years showed comparatively low UV levels.

On average, clouds reduce UV radiation at 345 nm by 22 – 43%, depending on time of the year. On rare occasions, reduction as high as 90% were observed. Cloud effects at PAL are larger than those observed at SPO[3] and MCM[4]. Our measurements indicate that clouds with an optical depth larger than 25 are frequently observed at PAL but are virtually absent at SPO. Time series of daily doses of spectral irradiance at 305 nm and of erythemal daily dose demonstrate large day-to-day and inter-annual variability during the austral spring (Figures 4 and 5). Variability is caused by difference in the depletion depth, timing, and location of the ozone hole. The variability due to changes in total ozone has been quantified by calculating departures from the climatological mean (Figure 7). During the first half of the year, the variability in UV introduced by clouds and albedo is about 2.5 times as high as that introduced by ozone. Between September and November, the variability introduced by ozone is similar to that caused by clouds.

ACKNOWLEDGMENTS

SUV-100 measurements at Palmer Station were supported by the National Science Foundation's Office of Polar Programs via subcontracts to Biospherical Instruments Inc. from Antarctic Support Associates (ASA) and Raytheon Polar Services Company (RPSC). We wish to express our gratitude to numerous operators of the SUV-100 spectroradiometer at Palmer Station. Ozone sonde measurements at Marambio were conducted by the National Meteorological Service of Argentina and data was obtained from the World Ozone and Ultraviolet Radiation Data Centre (WOUDC) at www.woudc.org. Atmospheric pressure and snow depth data from Palmer Station were provided by Matthew Lazzara, University of Wisconsin-Madison, and accessed via ftp://amrc.ssec.wisc.edu/pub/palmer/. We further thank R. D. McPeters and the Ozone Processing Team at NASA's Goddard Space Flight Center for providing TOMS total ozone and reflectivity data from toms.gsfc.nasa.gov.

REFERENCES

1. D. Lubin, J. E. Frederick, C. R. Booth, T. B. Lucas, and D. A. Neuschuler, "Measurements of enhanced springtime ultraviolet radiation at Palmer Station, Antarctica," *Geophys. Res. Lett*., **16**(8), 783-785, 1989.
2. C. R. Booth, T. B. Lucas, J. H. Morrow, C. S. Weiler, and P. A. Penhale, "The United States National Science Foundation's polar network for monitoring ultraviolet radiation", *Antarc. Res. Ser*., edited by C. S. Weiler and P. A. Penhale, **62**, 17-37, 1994.
3. G. Bernhard, C. R. Booth, and J. C. Ehramjian, "Version 2 data of the National Science Foundation's Ultraviolet Radiation Monitoring Network: South Pole," *J. Geophys. Res*., **109**, D21207, doi:10.1029/2004JD004937, 2004.
4. G. Bernhard, C. R. Booth, and J. C. Ehramjian, and S. E. Nichol, "UV climatology at McMurdo Station, Antarctica, based on Version 2 data of the National Science Foundation's Ultraviolet Radiation Monitoring Network," submitted to *J. Geophys. Res*., 2005.
5. B. Mayer, A. Kylling, "Technical note: The libRadtran software package for radiative transfer calculations – description and examples of use," *Atmos. Chem. Phys. Discuss*., **5**, 1319-1381, 2005.
6. C. A. Gueymard, "The sun's total and spectral irradiance for solar energy applications and solar radiation models," *Solar Energy*, **76**(4), 423-453, 2004.
7. R. L. Kurucz, , I. Furenlid, J. Brault, and L. Testerman, "Solar flux atlas from 296 to 1300 nm," National Solar Observatory Atlas No. 1, Harvard Univ. Press, Cambridge, Mass., 1984, available at ftp://ftp.noao.edu/fts/fluxatl/.
8. G. P. Anderson, S. A. Clough, F. X. Kneizys, J. H. Chetwynd, and E. O. Shettle, "AFGL atmospheric constituents profiles (0-120 km)," Tech. Rep. AFGL-TR-86-0110, Air Force Geophys. Lab., Mass., 1986.
9. G. Bernhard, C. R. Booth, and J. C. Ehramjian, "Comparison of measured and modeled spectral ultraviolet irradiance at Antarctic stations used to determine biases in total ozone data from various sources," in *Ultraviolet Ground- and Space-based Measurements, Models, and Effects*, edited by J. R. Slusser, J. R. Herman, and W. Gao, *Proc. SPIE*, **4482**, 115-126, 2002.
10. G.E. Shaw, "Atmospheric turbidity in the polar regions," *J. Appl. Meteorol*., **21**, 1080-1088, 1982.
11. G. Bernhard, C. R. Booth, and R. D. McPeters, "Calculation of total column ozone from global UV spectra at high latitudes," *J. Geophys. Res*., **108**(D17), 4532, doi:10.1029/2003JD003450, 2003.
12. A. Bass and R. J. Paur, "The ultraviolet cross sections of ozone: 1, The measurement," in *Atmospheric Ozone*, edited by C. Zerefos and A. Ghazi, pp. 606-616, D. Reidel, Norwell, Mass., 1985.
13. A. F. McKinlay and B. L. Diffey (Eds.), "A reference action spectrum for ultraviolet induced erythema in human skin," in *Commission International de l'Éclairage (CIE), Research Note*, **6**(1), 17-22, 1987.
14. R. B. Setlow, "The wavelength in sunlight effective in producing skin cancer: a theoretical analysis," *Proc. Natl. Acad. Sci. U.S.A*., **71**(9), 3363-3366, 1974.
15. J. Lenoble, A. Kylling, and I. Smolskaia, "Impact of snow cover and topography on ultraviolet irradiance at the Alpine station of Briancon," *J. Geophys. Res*., **109**, D16209, doi:10.1029/2004JD004523, 2004.
16. S. E. Nichol, G. Pfister, G. E. Bodeker, R. L. McKenzie, S. W. Wood, and G. Bernhard, "Moderation of cloud reduction of UV in the Antarctic due to high surface albedo," *J. Appl. Meteorol*., **42**(8), 1174-1183, 2003.
17. P. Ricchiazzi, C. Gautier, and D. Lubin, "Cloud scattering optical depth and local surface albedo in the Antarctic: simultaneous retrieval using ground-based radiometry," *J. Geophys. Res*., **100**(D10), 21,091-21,104, 1995.
18. World Meteorology Organisation (WMO), *Scientific assessment of ozone depletion: 2002*, Global ozone research and monitoring project, Report No. 47, 498 pp., Geneva, Switzerland, 2003.
19. M. J. Newchurch, E.-S. Yang, D. M. Cunnold, G. C. Reinsel, J. M. Zawodny, and J. M. Russell III, "Evidence for slowdown in stratospheric ozone loss: First stage of ozone recovery," *J. Geophys. Res*., **108**(D16), 4507, doi:10.1029/2003JD003471, 2003.